BIOCHEMISTRY
including biophysical chemistry & molecular biology
Article

Biochemistry **2010,** *49,* 8117–8126 8117
DOI: 10.1021/bi100865f

Identification of a Unique Ganglioside Binding Loop within Botulinum Neurotoxins C and D-SA[†,‡]

Andrew P.-A. Karalewitz,[§,@] Abby R. Kroken,[§,@] Zhuji Fu,[∥] Michael R. Baldwin,[⊥] Jung-Ja P. Kim,*[,∥] and Joseph T. Barbieri*[,§]

[§]*Department of Microbiology and of Molecular Genetics, and* [∥]*Department of Biochemistry, Medical College of Wisconsin, Milwaukee, Wisconsin 53226-3548, and* [⊥]*Department of Microbiology and Immunology, University of Missouri, Columbia, Missouri 65211* [@]*These authors contributed equally to this study.*

Received May 28, 2010; Revised Manuscript Received July 21, 2010

ABSTRACT: The botulinum neurotoxins (BoNTs) are the most potent protein toxins for humans. There are seven serotypes of BoNTs (A−G) based on a lack of cross antiserum neutralization. BoNTs utilize gangliosides as components of the host receptors for binding and entry into neurons. Members of BoNT/C and BoNT/D serotypes include mosaic toxins that are organized in D/C and C/D toxins. One D/C mosaic toxin, BoNT/D-South Africa (BoNT/D-SA), was not fully neutralized by immunization with BoNT serotype C or D, which stimulated this study. Here the crystal structures of the receptor binding domains of BoNT/C, BoNT/D, and BoNT/D-SA are presented. Biochemical and cell binding studies show that BoNT/C and BoNT/D-SA possess unique mechanisms for ganglioside binding. These studies provide new information about how the BoNTs can enter host cells as well as a basis for understanding the immunological diversity of these neurotoxins.

Botulinum neurotoxins (BoNTs)[1] are the most toxic proteins for humans (*1*). BoNTs are categorized into seven serotypes (A−G) based on neutralization characteristics where antiserum to one serotype will neutralize that serotype but not the other six serotypes. BoNTs are synthesized as 150 kDa proteins that possess AB structure−function organization, where A and B refer to individual domains within a protein toxin (*2*, *3*). BoNTs are cleaved by bacterial or host proteases into the two subunits, a light chain (LC, A for the activity domain) and a heavy chain (HC, B for the binding domain), that are linked by a disulfide bond (*4*). The LC has a mass of ∼50 kDa and possesses zinc-dependent protease activity (*5*), while the HC has a mass of ∼100 kDa and contains a receptor binding domain (HCR) and a translocation domain (HCT). The HCT is primarily α-helical with a disordered "belt" that wraps around the LC which may serve as a protease chaperone (*6*). The HCR comprises two structural subdomains, an N-terminal jellyroll motif and a C-terminal β-trefoil conformation.

BoNTs utilize dual receptors for entry into neurons (*7*). Upon delivery to a cholinergic nerve terminus, BoNT HCRs bind a ganglioside (*8*), which localizes BoNT to the neuronal plasma membrane. BoNTs then interact with a protein receptor to facilitate internalization. Host proteins that serve as BoNT receptors include the synaptic vesicle proteins, such as synaptic vesicle protein 2 (SV2) for BoNT/A, -E, and -F and synaptotagmin I/II for BoNT/B and -G (*9*−*13*). The host protein receptors for BoNT/C and BoNT/D remain to be determined. BoNT serotypes A, B, and E−G are internalized through synaptic vesicle recycling (*7*). How BoNT/C and -D enter neurons is not known. Upon acidification, the HCT inserts into the synaptic vesicle membrane and translocates the LC across the vesicle membrane into the cytosol where the LC (*14*, *15*) dissociates from the HC (*16*). BoNT LCs are zinc proteases that cleave neuronal soluble *N*-ethylmaleimide sensitive factor attachment protein receptor (SNARE) proteins. BoNT/A and -E cleave SNAP25. BoNT/B, -D, -F, and-G cleave synaptobrevin-2/vesicle associated membrane protein-2 (Syb-2/VAMP-2). BoNT/C cleaves SNAP25 and syntaxin 1 (*17*−*20*). Thus, BoNTs inhibit synaptic vesicle fusion and subsequent neurotransmitter signaling.

BoNT/C and BoNT/D are not typically associated with natural human infections (*21*). While BoNT/C does not appear to be toxic to humans following ingestion (*22*), BoNT/C is toxic for human tissues and cleaves SNAP25 and syntaxin in human neurons (*23*). BoNT/C was first isolated in 1922 and was shown to be responsible for botulism outbreaks that resulted in mass avian deaths (*24*−*26*). Mice deficient in complex ganglioside synthesis are resistant to BoNT/C toxicity, in agreement with a direct interaction being observed between BoNT/C and gangliosides GD1b and GT1b (*27*). Conversely, BoNT/C is not believed to utilize a synaptic vesicle protein for neuron entry, and high-affinity binding of BoNT/C to cell lysates is insensitive to proteinase K (*27*−*29*). In contrast, BoNT/D does not bind gangliosides but binds derivatives of phosphatidylethanolamine (*27*).

[†]J.T.B. and J.-J.P.K. acknowledge membership and support from the National Institutes of Health Regional Center of Excellence for Biodefense and Emerging Infectious Diseases Research Program, Great Lakes Regional Center of Excellence Grant 1-U54-AI-057153. M.R.B. is supported by National Institute of Neurological Disorders and Stroke Grant NS061763.

[‡]Coordinates have been deposited as Protein Data Bank entries 3N7K for HCR/C, 3N7J for HCR/D, 3N7L for HCR/D-SA, and 3N7M for HCR/D-SA-W1252A.

*To whom correspondence should be addressed. J.T.B.: phone, (414) 955-8412; e-mail, jtb01@mcw.edu; fax, (414) 944-8412. J.-J.P.K.: phone, (414) 955-8479; e-mail, jjkim@mcw.edu.

[1]Abbreviations: BoNT, botulinum neurotoxin; HCR, heavy chain receptor binding domain of BoNT; VAMP2, vesicle-associated membrane protein 2; SNAP25, synaptosomal-associated protein of 25 kDa; SNARE, soluble NSF attachment receptors; PDB, Protein Data Bank; rmsd, root-mean-square deviation.

Published on Web 07/26/2010

In addition to the prototype toxins, BoNT/C and BoNT/D mosaics (D/C and C/D) exist and include BoNT/D-South Africa (BoNT/D-SA), a D/C mosaic toxin. Mice immunized with the BoNT/C HCR were only partially protected from challenge by BoNT/D-SA, and immunization with the BoNT/D HCR did not protect mice from BoNT/D-SA challenge (*30*).

To initiate studies to define why vaccination with HCR/C or HCR/D did not provide complete protection against challenge by BoNT/D-SA, we determined the crystal structures of BoNT/C, BoNT/D, and BoNT/D-SA. This allowed identification of a unique mechanism for ganglioside binding by BoNT/C and BoNT/D-SA. In addition, we determined the structure of a mutated form of HCR/D-SA, W1252A, which has a decreased affinity for ganglioside binding.

EXPERIMENTAL PROCEDURES

Materials. *Escherichia coli* codon-optimized DNAs encoding the HCR domains of BoNT/C-Stockholm (residues 864−1290), BoNT/D-1873 (residues 861−1276), and BoNT/D-South Africa-5995 (residues 867−1285) were synthesized by EZBiolab (Westfield, IN). Chemicals and reagents were obtained from Sigma-Aldrich Co. (St. Louis, MO), and restriction enzymes were purchased from New England Biolabs (Ipswitch) or Invitrogen (Carlsbad, CA). Sprague-Dawley rat embryonic day 18 cortical neurons were purchased from Brainbits LLC (Springfield, IL) and cultured as described by the supplier. Neuronal cell culture reagents were purchased from Invitrogen.

Expression and Purification of BoNT HCRs. DNA encoding HCRs were subcloned into pET-28a (Novagen) which introduced a 3-FLAG eiptope N-terminal to the HCR. HCRs were purified from *E. coli* BL-21(DE3) cells using three sequential steps: Ni^{2+}-nitrilotriacetic acid chromatography, S200-HR gel filtration chromatography, and DEAE-Sephacryl ion exchange chromatography. Typical purifications from a 1 L culture yielded between 5 and 10 mg of the HCR. Mutated forms of HCR/C and HCR/D-SA were prepared using a Quikchange site-directed mutagenesis kit (Stratagene).

HCR−Ganglioside Binding Assay. Binding of the HCR to gangliosides was assessed in a solid phase assay as previously described (*31*). Briefly, bovine brain gangliosides (Matreya, LLC) were stored in dimethyl sulfoxide (20 mg/mL) at −20 °C, diluted into methanol, and applied to non-protein binding 96-well plates (Corning Costar catalog no. 3641) at 0.5 or 2.0 μg of gangliosides/well. MeOH was evaporated at room temperature (RT), and the wells were washed three times with phosphate-buffered saline (PBS). Plates were blocked with 2% BSA in sodium carbonate buffer [50 mM Na_2CO_3 (pH 9.6)] for 1 h. Binding assays were performed in 100 μL of PBS per well for 2 h at 4 °C containing the indicated HCR at 10 nM. The bound HCR was detected with an α-FLAG M2 monoclonal antibody conjugated to horseradish peroxidase (HRP, diluted 1/10000, Sigma-Aldrich) and detected using TMB-Ultra (Pierce Biochemicals) as the substrate. The reaction was stopped with 1 M H_2SO_4, and the absorbance at 450 nm was determined using a plate reader (Victor 3 V, Perkin-Elmer).

HCR−Cell Binding Assays. Primary rat cortical neurons were plated and cultured in 24-well glass bottom culture dishes precoated with poly-D-lysine and laminin (Sigma-Aldrich and Thermo Fisher Scientific, Wyman, MA). Following 10−14 days, neurons were cooled with two washes in cold PBS and incubated with a dilution series of the indicated HCR in neurobasal medium for 1 h at 4 °C. Cells were washed and processed for microscopy. Briefly, fixation in 4% paraformaldehyde in PBS (15 min at RT) was followed by incubation with 150 mM glycine in PBS. Nonspecific binding sites were blocked with 10% fetal calf serum, 2.5% fish skin gelatin (Sigma-Aldrich), 0.1% Triton X-100 (Sigma-Aldrich), and 0.05% Tween 20 (EMD Chemicals, Gibbstown, NJ) in PBS for 1 h at RT. Cells were incubated overnight with an α-FLAG M2 mAb (diluted 1/15000, Sigma-Aldrich) followed by goat α-mouse IgG-488 (diluted 1/500, Invitrogen) in PBS for 1 h at RT. Following washing and fixation, samples were mounted in AF3 antifade reagent (Electron Microscopy Sciences, Hatfield, PA). Images were captured on an Eclipse TE2000 inverted microscope (Nikon Instruments Inc., Melville, NY) equipped with a CFI Plan Apo VC 60× oil, NA 1.4-type objective and Cool Snap HQ2 camera (Photometrics, Tuscon, AZ). The average 3xFLAG fluorescence intensity from five random fields was determined and corrected for background fluorescence by subtraction of the signal from a minus HCR control sample. The fluorescence signal was analyzed using MetaMorph (Molecular Devices, Sunnyvale, CA). Data were presented using GraphPad Prism (GraphPad Software, Inc., La Jolla, CA) and represent the average of two independent experiments.

Crystallization and Data Collection. Purified HCR proteins were dialyzed and concentrated to 5 mg/mL in buffer containing 20 mM Tris-HCl (pH 7.6) and 100 mM NaCl. Crystals were produced by vapor diffusion using a hanging drop containing 2 μL of a protein solution mixed with 2 μL of a well solution consisting of 0.1 M MES (pH 6.5), 12% PEG 20K, and 0.5 M NaCl for HCR/C; 0.1 M Hepes (pH 7.5), 10% PEG 8K, and 8% ethylene glycol for HCR/D; 0.1 M MES (pH 6.0), 5% PEG 400, 1.8 M ammonium sulfate, and 250 mM NaCl for HCR/D-SA; and 0.1 M Hepes (pH 7.5), 4% PEG 400, and 45% ammonium sulfate for the W1252A mutant of HCR/D-SA (HCR/D-SA-W1252A). Diffraction data for HCR/D-SA and HCR/D-SA-W1252A were collected at 100 K at beamline SBC 19ID of the Advanced Photon Source (Argonne National Laboratory, Argonne, IL), and data for HCR/C and HCR/D were collected using an R-AXIS IV^{++} instrument with a MicroMax 007 generator at 100 K. HKL2000 (*32*) was used for data processing. Data collection and processing statistics for all crystals are summarized in Table 1.

Structure Determination and Refinement. The structure of HCR/D was determined by the molecular replacement method using MOLREP within the CCP4 (*33*) program suite and using the structure of HCR/A [residues 875−1295, PDB entry 3FUO (*13*)]. The structure of HCR/C was determined using HCR/D, the structure of HCR/D-SA with HCR/C, and the structure of HCR/D-SA-W1252A with HCR/D-SA. Initial structures obtained from the molecular replacement trials were refined using CNS (*34*). The refinement procedure consisted of rigid body and positional refinements followed by a simulated annealing protocol. Iterative rounds of positional and temperature factor refinement were followed by manual fitting and rebuilding using TURBO-FRODO (*35*) with $2|F_o| - |F_c|$ and $|F_o| - |F_c|$ difference Fourier maps. At later stages of refinement, water molecules were assigned where electron densities were greater than 3σ in the $|F_o| - |F_c|$ map and situated within 3.3 Å of a potential hydrogen bonding partner. The final models were completed with $R_{crystal}$ and R_{free} values of 0.192 and 0.254 for HCR/C, 0.221 and 0.256 for HCR/D, 0.216 and 0.257 for HCR/D-SA, and 0.222 and 0.270 for HCR/D-SA-W1252A, respectively (Table 1).

Table 1: Data Collection and Refinement Statistics

	HCR/C (PDB entry 3N7K)	HCR/D (PDB entry 3N7J)	HCR/D-SA (PDB entry 3N7L)	HCR/D-SA-W1252A (PDB entry 3N7M)
		Data Collection		
resolution range (Å)	30−2.5/2.54−2.50	30−2.0/2.07−2.0	30−2.0/2.03−2.0	30−2.6/2.69−2.6
total no. of reflections	171070	486972	246215	100450
no. of unique reflections	45896/1679	35231/2793	41661/1610	19457/1861
completeness (%)	90.9/67.5	95.2/77.2	97.4/77.7	99.0/97.1
redundancy	3.7/2.1	13.8/7.3	5.9/4.4	5.2/4.5
$I/\sigma(I)$	8.3/1.9	26.8/2.7	18.4/2.6	15.5/2.5
unit cell dimensions				
a, b, c (Å)	98.2, 77.4, 107.4	60.0, 94.2, 95.0	57.3, 57.8, 184.2	57.4, 57.8, 184.7
β (deg)	116.36	90	90	90
space group	$P2_1$	$P2_12_12_1$	$P2_12_12_1$	$P2_12_12_1$
R_{symm}	0.105/0.330	0.090/0.497	0.086/0.434	0.098/0.526
V_m (Å^3/Da)/solvent content (%)	3.6/65	2.7/52	3.0/58	3.1/58
no. of monomers per asymmetric unit	2	1	1	1
		Refinement		
$R_{crystal}/R_{free}$[a]	0.192/0.254[b]	0.221/0.256	0.216/0.257	0.222/0.270
rmsd for bond lengths (Å)	0.008	0.006	0.006	0.007
rmsd for bond angles (deg)	1.4	1.3	1.4	1.5
no. of protein atoms	6919	3335	3412	3403
no. of water molecules	110	179	169	56
no. of sulfate/glycerol atoms			15/36	5/6
average B factor (Å^2)				
main chain atoms	30.4	40.9	29.4	39.9
side chain atoms	30.4	43.8	32.0	40.0
water molecules	24.1	46.7	35.4	57.1
sulfate/glycerol molecules			54.6/46.2	38.9

[a]Without using Twin-Fraction and Twin-Operator, $R_{crystal}$ and R_{free} equal 0.221 and 0.276, respectively. [b]Twin-Operator: $-h, -k, h + l$; Twin-Fraction = 0.113.

Table 2: Amino acid Identity of BoNT/C and BoNT/D with BoNT/D-SA

	% identity to BoNT/D-SA domains[A]			
	light chain (residues 1−447)	translocation (residues 447−866)	HCR_N (residues 867−1084)	HCR_C (residues 1085−1285)
BoNT/A1	33	36	36	31
BoNT/C	47	70	90	62
BoNT/D	98	95	50	24

[A]BoNT/A1 Hall ATCC 3502 (5185061), BoNT/C1 Stockholm (D90210 YP_398516), and BoNT/D CB16 D-1873 (S49407, ZP_04863672) were aligned with BoNT/D-South Africa (EF378947, S70582). Residues are indicated relative to BoNT/D-SA. Identity was determined by ClustalW2 sequence alignment algorithm.

RESULTS

Amino Acid Sequence Alignment of BoNT HCR/C, HCR/D, and HCR/D-SA. The percent amino acid identities of BoNT/A, BoNT/C, and BoNT/D relative to BoNT/D-SA are listed in Table 2. BoNT/D-SA is a mosaic neurotoxin composed of the LC and HCT of BoNT/D and a receptor binding domain (HCR) that resembles BoNT/C as previously described (*36*). The low identity within the C-terminal subdomain (62%) relative to the identity between the N-terminal subdomains (90%) of the respective HCRs of BoNT/D-SA and BoNT/C indicates genetic drift since the generation of the mosaic gene. The significance of this divergence was defined by Smith and co-workers who reported that vaccination with either HCR/C or HCR/D failed to yield complete protection against challenge by BoNT/D-SA (*30*). These observations stimulated the characterization of the structure−function properties of the HCRs of BoNT/C, BoNT/D, and BoNT/D-SA.

Structures of the HCR from BoNT/C, BoNT/D, and BoNT/D-SA. The crystal structures of HCR/C, HCR/D, and HCR/D-SA were determined and shown to have an overall conservation of structure (Figure 1A) among each other as well as among other serotypes of BoNTs (*3*, *37*−*39*). The HCRs are organized with an N-terminal jellyroll motif and a C-terminal β-trefoil conformation. Overall, the structures of HCR/D-SA and HCR/D have an rmsd of 2.5 Å, and HCR/D-SA and HCR/C have an rmsd of 0.5 Å. The angle between the N- and C-terminal subdomains of HCR/D is more obtuse than that observed between the two subdomains in HCR/C and HCR/D-SA. This change in angle did not appear to be due to changes in crystal packing and likely perturbed the calculated rmsd values for the entire HCR. The calculated rmsd values between the individual subdomains of HCR/D and HCR/D-SA were determined to be 1.5 Å for the N-terminal domain and 3.6 Å for the C-terminal domain. When the rmsd was determined between the C-terminal subdomain of HCR/D and HCR/D-SA excluding loops, the

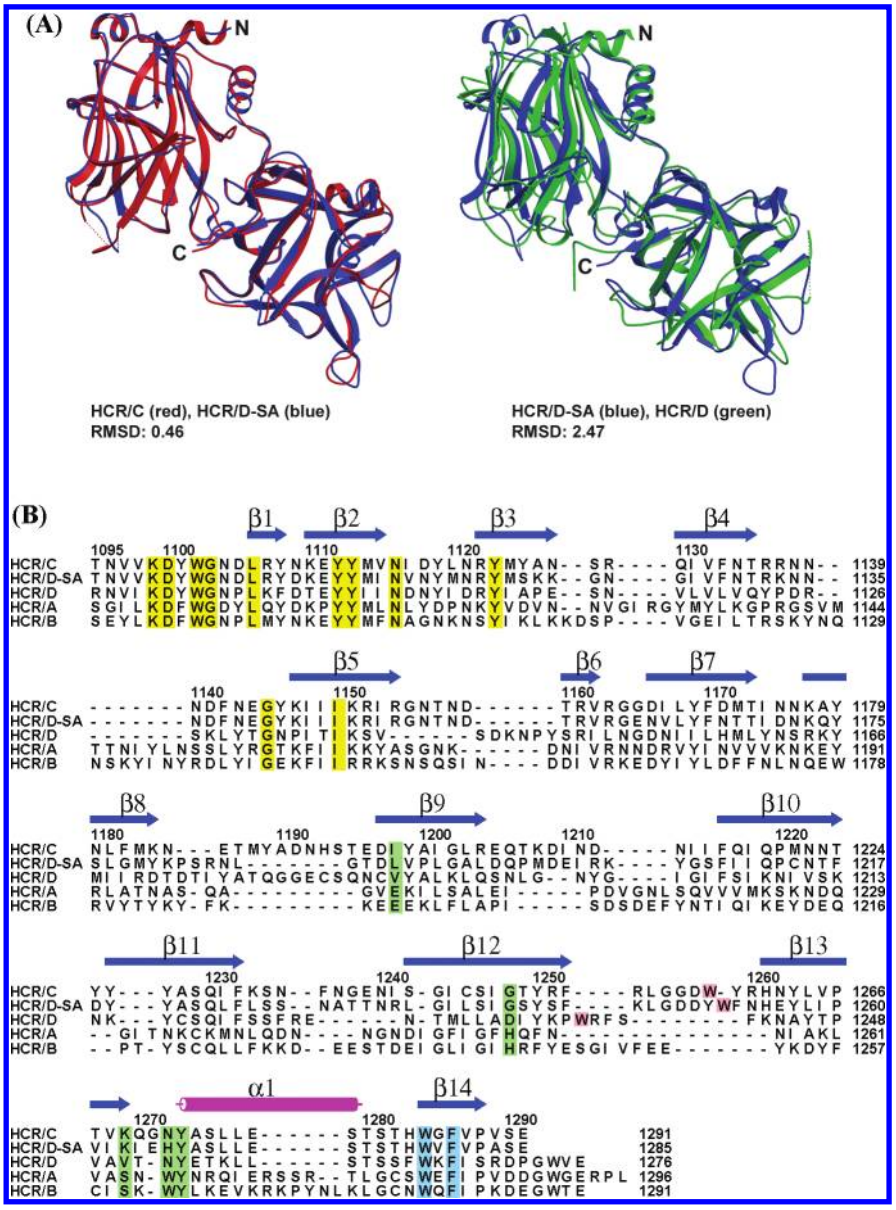

FIGURE 1: Crystal structures of HCR/C, HCR/D, and HCR/D-SA. (A) Shown are overlays of the crystal structure of HCR/D-SA (blue) with HCR/C (left panel, red) (rmsd = 0.46) and HCR/D-SA (blue) with HCR/D (right panel, green) (rmsd = 2.47). (B) Structure-based alignments of the C-terminal subdomains of HCR/C, HCR/D, and HCR/D-SA with HCR/A and HCR/B shown. β-Strands, α-helices, and loops are numbered from residue 1095 of HCR/C. Internal W and F (W1278 and F1280 of HCR/D-SA) (highlighted in blue) were conserved among the HCRs and provided a point of reference for the alignment. Residues within the ganglioside binding domain of HCR/A are colored green (E, H, S, W, and Y). Tryptophans within the ganglioside binding loop of HCR/C (W1258) and HCR/D-SA (W1252) are colored pink. A W, located at a different position in the analogous region of the GBL of HCR/D (W1238), is colored pink. Yellow residues represent conserved amino acids within the HCRs that have not been associated with ganglioside or receptor binding functions.

value was found to be 1.8 Å, indicating that the majority of structural divergence is in the loop regions of the C-terminal subdomain. The primary divergence of structure within HCR/D-SA and HCR/C was within the loops of the C-terminal subdomain, which includes the ganglioside binding pocket that has been described for several other BoNT serotypes (*39*).

Structure-Based Alignments of HCR/C, HCR/D, and HCR/D-SA. The crystal structures were used to construct a structure-based amino acid sequence alignment (Figure 1B), with HCR/A and HCR/B as references. C-Terminal, buried W (W1278 for HCR/D-SA) and F (F1280 for HCR/D-SA) are structurally conserved among the HCRs and served as a reference point for the alignment. As the main chain of the HCRs proceeds from the buried W-F pair toward the N-terminus, the peptide emerges from the interior and assumes a helical conformation. This helix constitutes part of the ganglioside binding pocket (GBP) (Figure 2) observed for BoNT/A, -B, -E, -F, and -G and comprises several conserved residues that define the boundaries of the pocket (*40*). Y1267 and W1266 of HCR/A are present on the N-terminal side of the helix and contribute to ganglioside binding, while S1264 in the vicinity of the helix and E1203 also participate in ganglioside binding (*40*). The main chain of the HCRs continues toward the N-terminal domain and forms a β-hairpin loop that continues into an antiparallel β-sheet that forms the adjacent side of the GBP located opposite W1266 and contains a H which participates in ganglioside binding (H1253 of HCR/A). BoNT/B displays a GBP structurally identical to that observed in BoNT/A. Interestingly, the β-loop formed by the antiparallel β-strands which make up one side of the GBP is composed of 10 amino acids rather than a shorter four-residue loop that is present in HCR/A.

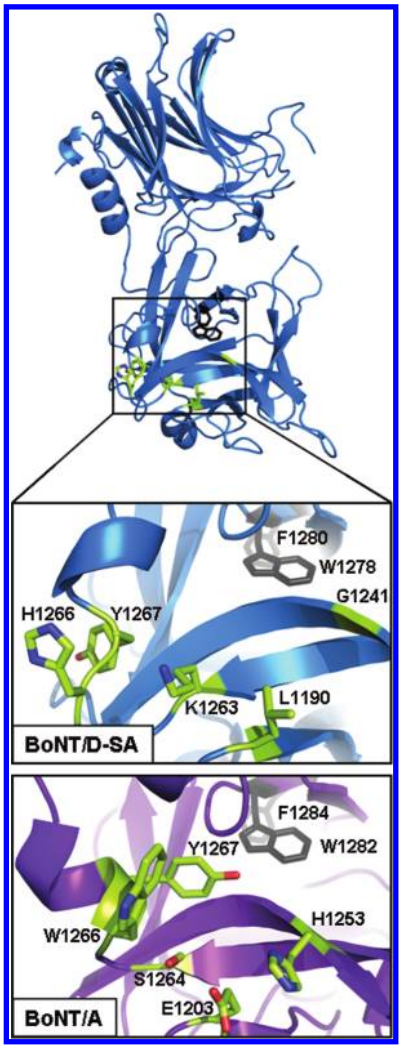

FIGURE 2: Overlay of the ganglioside binding pocket of HCR/A with the representative residues of HCR/D-SA. HCR/D-SA (blue) is shown with the following highlighted residues: conserved internal F1280 and W1282 (gray) and corresponding residues that represent the ganglioside binding pocket of HCR/A (green). The ganglioside binding pocket of HCR/A (bottom) and the corresponding region of HCR/D-SA (top) were expanded and are shown. Residues that contribute to ganglioside binding of HCR/A (E1203, H1253, S1264, W1266, and Y1267) and corresponding residues within HCR/D-SA that align in space are colored green, with nitrogen and oxygen atoms colored blue and red, respectively. This alignment indicates the major determinant of ganglioside binding, a conserved tryptophan residue present in the ganglioside binding pocket of BoNT/A, -B, -E, -F, and -G, and TeNT is absent from the structurally analogous region of HCR/D-SA.

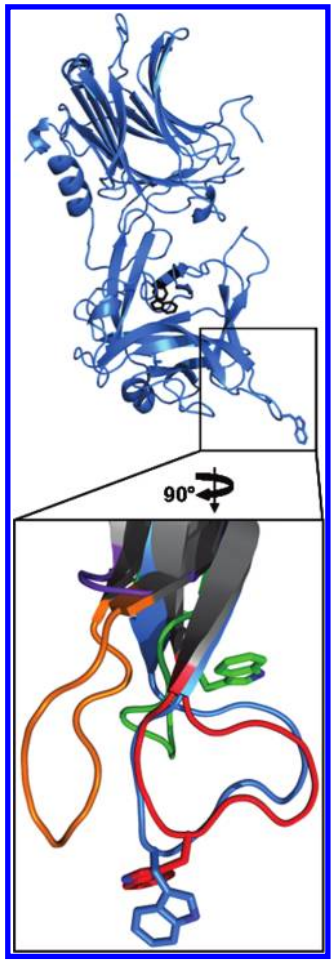

FIGURE 3: Overlay of the ganglioside binding loops of HCR/C, HCR/D, and HCR/D-SA with the representative loops of HCR/A and HCR/B. HCR/D-SA (blue, top) is shown with the conserved, buried F1280 and W1282 (black), and the ganglioside binding loop (GBL) W1252 indole ring is also shown at the tip of the loop. The GBL was enlarged, rotated, and shown (lower) aligned with the structurally analogous β-hairpin loops of BoNT/A (purple), BoNT/B (orange), BoNT/C (red), and BoNT/D (green). HCR/C and/D-SA loops display a similar overall structural arrangement with the indole ring of the W residue implicated in ganglioside binding [HCR/C (W1258) and HCR/D-SA (W1252)] extending away from the HCR molecule. HCR/D, like HCR/C and/D-SA, has a tryptophan residue (W1238) in the β-hairpin loop. However, unlike HCR/C and/D-SA, the HCR/D W1238 indole ring does not extend away from the HCR but rather is oriented toward an adjacent β-hairpin loop. BoNT/B has an extended β-hairpin loop like HCR/C, -D, and -D-SA but lacks a tryptophan residue. BoNT/A, in contrast, does not have an extended β-hairpin loop.

The crystal structures of HCR/C, HCR/D, and HCR/D-SA display an overall structural similarity to HCR/A and HCR/B (Figure 1A) that includes the buried W and F residues where the main chain proceeds from the interior to an α-helix that is structurally analogous to the GBP of HCR/A. However, within this analogous region, neither HCR/D-SA, HCR/D, nor HCR/C contains the conserved W, S, or H, and the phenolic ring of Y is oriented away from the pocket. Proceeding from the GBP, HCR/C, HCR/D, and HCR/D-SA also form β-loops [between β12 and β13 (see Figure 1B)] similar in size to HCR/B and contain a W that was determined to contribute to the binding of HCR/C and HCR/D-SA to gangliosides, as shown below. This loop will be termed the ganglioside binding loop (GBL) (Figure 3).

Ganglioside Binding by HCR/C and HCR/D-SA. The ability of the HCRs to bind gangliosides was investigated in a solid phase binding assay. Previous studies showed that HCR/C bound GD1b and GT1b (*27*) . Complex gangliosides were immobilized in 96-well plates, and 10 nM HCRs were added to each ganglioside well. HCR/TeNT was used as a control to demonstrate effective ganglioside immobilization as HCR/TeNT binds b-series gangliosides with high affinity (*41*). HCR/C bound GD1b with the highest affinity, followed by GT1b, GD1a, and GM1a, while HCR/D-SA displayed a unique binding preference for GM1a, followed by GD1a with a lower affinity for b-series gangliosides (Figure 4). Thus, HCR/C and HCR/D-SA have unique preferences for gangliosides, and the preferred binding of HCR/D-SA to GM1a is a unique property among the BoNT serotypes.

Role of Tryptophan within the Ganglioside Binding Loop (GBL) in HCR/C and HCR/D-SA Binding to Gangliosides.

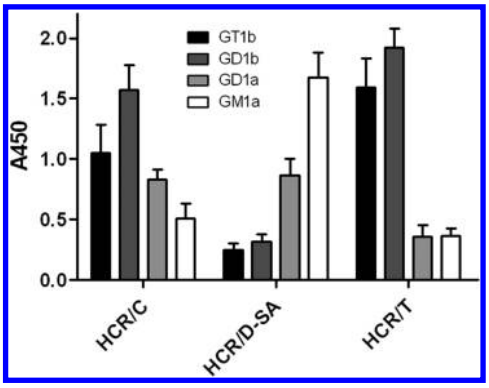

FIGURE 4: HCR/C and HCR/D-SA binding to complex gangliosides. Wells (96-well plates) were coated with the indicated ganglioside (0.5 μg per well in 100 μL of MeOH). Plates were dried, and 10 nM HCR/C, HCR/D-SA, or HCR/T was incubated in 100 μL of PBS for 1 h at 4 °C. Wells were washed, and bound HCR was detected with an anti-FLAG-HRP antibody followed by TMB-Ultra. A_{450} was determined as the average of three independent experiments.

Ganglioside binding experiments were conducted to determine the role of the W within the GBL of HCR/C(W1258A) and HCR/D-SA(W1252A) for binding of the HCR to GD1b and GM1a, respectively. Previous studies showed that HCR/C utilized W1258 for cell binding (*42*). Gangliosides were immobilized on a 96-well plate, and HCRs and the mutated HCRs were tested for ganglioside binding affinity. HCR/C bound GD1b in a dose-dependent manner, while the level of binding of HCR/C(W1258A) to GD1b was reduced (Figure 5). In a similar experiment, HCR/D-SA bound GM1a in a dose-dependent manner, while the level of HCR/D-SA(W1252A) binding was reduced (Figure 5). These experiments supported the role of the W within the GBL as contributing to the coordination of ganglioside binding by HCR/C and HCR/D-SA. The crystal structure of the GBL of HCR/D-SA(W1252A) is identical to that of HCR/D-SA (Figure 6), indicating that the W1252A mutation does not cause structural perturbation to secondary sites on the HCR.

Role of the Tryptophan within the GBL in HCR/C and HCR/D-SA Binding to Primary Neurons. W1258 or W1252 within the GBL of HCR/C or HCR/D-SA, respectively, was tested for its ability to coordinate binding of the HCR to the plasma membrane of neurons by measuring the binding of HCRs to primary cortical neurons at 4 °C. HCR/A did not exhibit detectable binding to neurons at 4 °C, consistent with the need for synaptic vesicle fusion to expose the protein receptor (C. Chen and J. T. Barbieri, manuscript submitted for publication), SV2, while HCR/T showed a dose-dependent binding to neurons at 4 °C consistent with HCR/T utilizing gangliosides present in the outer leaflet of the plasma membrane as receptors for entry into neurons as previously described (*31*). Both HCR/C and HCR/D-SA bound to neurons in a dose-dependent manner (Figure 7A), with binding observed over the cell body as well as on extended appendages. HCR/D-SA had a lower overall fluorescence intensity relative to HCR/C. In contrast, HCR/D did not show detectable neuron binding above background. Neither HCR/C(W1258A) nor HCR/D-SA(W1252A) bound neurons above background. Figure 7B quantifies the dose-dependent binding pattern of the HCRs. These data indicate HCR/C and HCR/D-SA bind neurons through receptors localized to the plasma membrane and that binding is coordinated by the W within the GBL, while HCR/D did not show detectable binding above that observed for HCR/A.

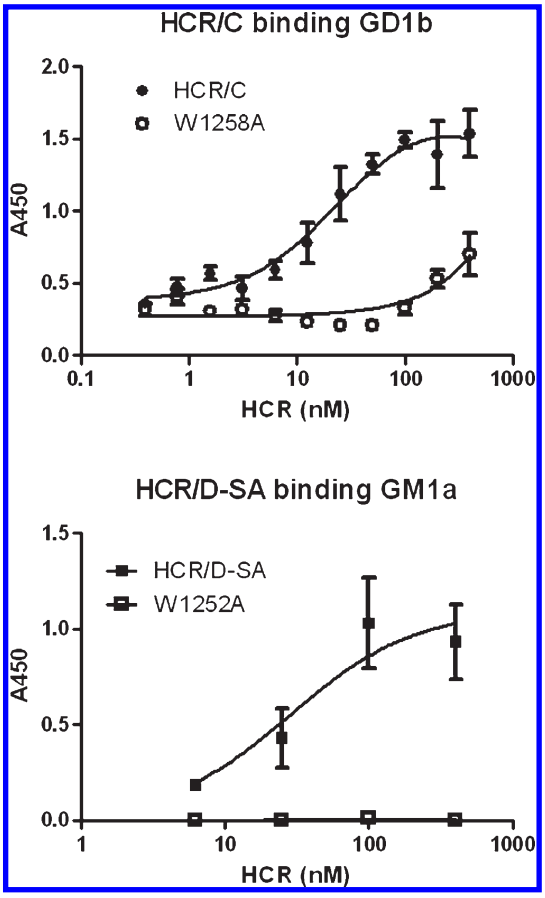

FIGURE 5: Role of tryptophan within the ganglioside binding loop in HCR/C and HCR/D-SA binding to complex gangliosides. Wells (96-well plates) were coated with GD1b (top) or GM1a (bottom) [0.5 μg (HCR/C) or 2.0 μg (HCR-D-SA) per well in 100 μL of MeOH]. Plates were dried, and 10 nM HCR/C or HCR/C(W1258A) (top) or HCR/D-SA or HCR/D-SA(W1252A) (bottom) was incubated in 100 μL of buffer for 1 h at 4 °C. Bound HCR was detected with an M2 anti-FLAG antibody followed by TMB-Ultra. A_{450} was determined and plotted as the average of at least duplicate determinations. The background absorbance of HCR bound to the well in the absence of the ganglioside was subtracted to account for nonspecific binding. No binding above background was detected for HCR/D-SA-(W1252A) so these values are presented as zero.

DISCUSSION

Structures of HCR/C, HCR/D, and HCR/D-SA. The crystal structures of HCR/C and HCR/D possess an overall structural homology with those of other BoNT HCR serotypes, with the N-terminal subdomain adopting a jellyroll motif and the C-terminal subdomain composed primarily of loops that are organized in a β-trefoil conformation. Nuenket et al. recently reported crystallization of HCR/D-SA; however, no structural solution was reported (*43*). In agreement with the primary amino acid sequence alignment, the structure of HCR/D-SA displayed a higher degree of structural similarity to the N-terminus of HCR/C than that of HCR/D. There are limited regions of homology within the loops of the C-terminal β-trefoil domain of HCR/D-SA and HCR/C, which is consistent with HCR/C and HCR/D-SA possessing unique ganglioside binding profiles. While the contribution of the GBLs of HCR/C and HCR/D-SA to ganglioside binding is unique, HCR/B shares a β-loop with the GBLs of HCR/C and HCR/D-SA (Figure 1B). The β-loop in HCR/B does not contribute to ganglioside binding and lacks a W; Stevens and co-workers proposed that the β-loop in HCR/B contributes to membrane binding through hydrophobic interactions (*38*).

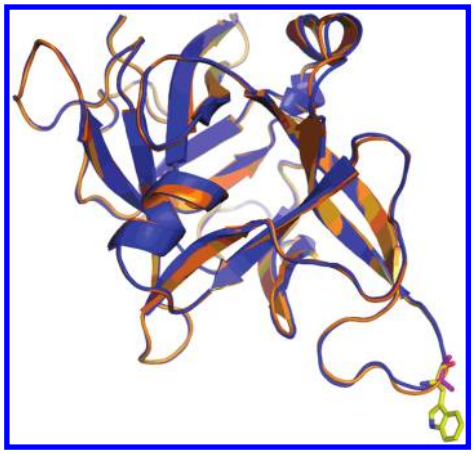

FIGURE 6: Crystal structure of HCR/D-SA(W1252A). Overlay of the crystal structures of the C-terminal subdomains (residues 1091−1285) of HCR/D-SA(W1252A) (orange) and HCR/D-SA (blue). The indole ring (yellow) of W1252 of HCR/D-SA and the methyl group (pink) of A1252 of HCR/D-SA(W1252A) are also shown.

Conversely, the homologous loop in BoNT/A is short, approximately four amino acid residues, which may preclude the loop from inserting into the cell membrane.

Ganglioside Binding Pocket. BoNT/A, -B, -E, -F, and -G contain a ganglioside binding pocket (GBP) (Figure 2) that is conserved by sequence identity (H...SXWY, except in serotype G where H is replaced with G and serotype E where H is replaced with K) and structural alignment (*44*). In HCR/A, H1253 is located on the first β-strand (β12) that makes up the final β-hairpin in the C-terminal domain of the HCR. The peptide continues through the β-hairpin conformation and turns back forming an antiparallel β-sheet ending in S1264, followed by a short α-helix, which contains W1266 and Y1267 (BoNT/A residue nomenclature). These residues (H1253, S1264, W1266, and Y1267) together with E1203 form a "pocket" for ganglioside binding. The imidazole ring of H and the indole ring of the W are perpendicular to each other within the GBP, while the Y and S form the back wall of the GBP. In a cocrystal structure of BoNT/A with GT1b, galactose sugar ring 4 of the ganglioside backbone sat parallel to the indole ring of W and interacted through a hydrophobic ring stacking mechanism. The interaction was further stabilized by contacts with E1203, H1253, and S1264. While the overall main chain organization of the GBP is present in HCR/C, HCR/D, and HCR/D-SA, the residues that contact ganglioside have been substituted, precluding ganglioside binding within the GBP of HCR/C and/D-SA. This conclusion is based upon the observation that HCR/C(W1258A) and HCR/D-SA(W1252A) were defective for ganglioside binding (Figure 2). HCR/C, -D, and -D-SA lacked H, W, and S, and the Y on the N-terminal side of the α-helix is in a different position relative to HCR/A with the phenolic ring oriented away from the pocket. Moreover, the structure and position of the α-helix that defines the GBP are not conserved in HCR/C and HCR/D-SA relative to HCR/A. Thus, the GBP in HCR/C, HCR/D-SA, and HCR/D has a different architecture and slightly different location and orientation compared to those of the GBP of HCR/A.

Ganglioside Binding Loop. Earlier studies showed that BoNT/C toxicity was dependent on complex gangliosides (*27*, *29*). We confirmed the ability of BoNT/C to bind b-series gangliosides and demonstrated that HCR/D-SA bound GM1a. Thus, HCR/C and HCR/D-SA utilize a unique ganglioside binding loop (GBL)

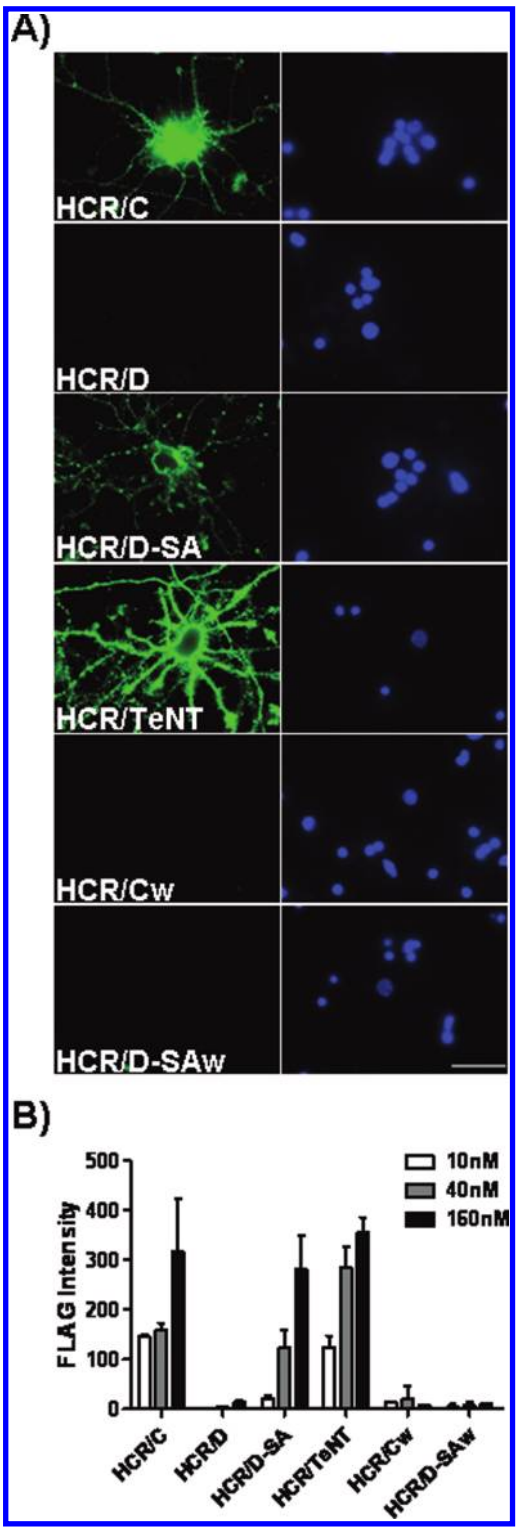

FIGURE 7: Binding of HCR/C, HCR/D, and HCR/D-SA to primary cortical neurons. Primary cortical neurons were plated and cultured in 24-well glass bottom culture dishes coated with poly-D-lysine and laminin. Following 10 days of culture, cells were washed and incubated with a dilution series of the indicated HCR in medium for 1 h at 4 °C. Bound HCR was identified by immunofluorescence microscopy using a mouse anti-Flag mAb followed by goat anti-mouse IgG-488. (A) Representative images of the indicated HCR (40 nM) bound to neurons (left panels) and nuclei stained with Hoechst (right panels) are shown (60× magnification). Images were captured at identical exposure times and analyzed using Image J. The scale bar is 35 μm. (B) Quantification of HCR binding to neurons. The values presented are arbitrary fluorescence units and represent the average FLAG fluorescence intensity from five random fields following correction for nonspecific fluorescence. The average of two independent experiments is shown.

(Figure 3) located more than 20 Å from the ganglioside binding pocket present in other BoNT serotypes. In the structure-based alignment, HCR/C and HCR/D-SA possess a homologous W within the GBL. Tsukamoto and colleagues reported that mutation of the W1258 to A weakened the ability of the HCR to compete with BoNT/C for synaptosome binding (*42*); here we show that this W contributes to ganglioside binding.

While each BoNT serotype contains a loop that corresponds to the GBL, the loops vary in size and composition. HCR/A has a β-finger (i.e., a two-residue loop) with several hydrophobic residues toward the end of the finger followed by the two consecutive N residues at the tip of the finger which is exposed to solvent. On the other hand, HCR/B has a loop more structurally analogous to that of HCR/C and HCR/D-SA, but lacking a W. The GBLs of BoNT/C and BoNT/D-SA represent a gain of function of ganglioside binding with a loss of function at the prototypical ganglioside binding pocket.

BoNT/C and BoNT/D-SA have different ganglioside specificities despite structurally similar binding sites. HCR/C interacted with b-series ganglioside GD1b, while HCR/D-SA preferred binding to a-series ganglioside GM1a. The neuronal cell binding experiment supported this observation, since the neuronal plasma membrane is enriched primarily in b-series gangliosides and has lower levels of a-series gangliosides. As a result, HCR/D-SA would be expected to have fewer binding sites on primary cortical neurons than HCR/C or HCR/T. The W within the GBL of HCR/D is located closer to the main body of the HCR (Figure 3), which may interfere with the ability to bind gangliosides (*42*).

The overlap of the W locations within the GBL of HCR/C and HCR/D-SA indicates that while W is required for ganglioside binding, this residue does not contribute to specificity. Thus, other residues within the GBL may contribute to ganglioside binding specificity. The protein structure of HCR/D-SA-(W1258A) is unchanged with respect to the wild-type protein which argues that the W in the GBL contributes directly to ganglioside binding. HCR/C has two R residues flanking either side of the loop (R1251 and R1260) and R1253 near the W, which may provide contacts for sialic acid residues in b-series gangliosides. The GBL of HCR/D-SA contains an additional D (D1249), which may repel the sialic acid carboxylates of b-series gangliosides. Further studies will be conducted to determine which residues make contact with gangliosides and how gangliosides interact with this novel GBL.

Several other bacterial toxins bind ganglioside receptors but utilize different mechanisms of binding. For example, the heat-labile enterotoxins of *E. coli* as well as cholera toxin also use a tryptophan residue to coordinate sugar binding, as demonstrated by structure and mutagenesis studies (*45*, *46*). However, the binding sites are generated by interactions of two subunits of the B-pentamer, as opposed to the β-trefoil conformation adopted by BoNTs and TeNT. The neuraminidase of influenza virus binds sialic acid by a mechanism lacking a tryptophan residue contact (*47*). In addition, the eukaryotic lectins have been described, including ricin toxin, *Sambucus nigra* agglutinin II, EW29 from the earthworm *Lumbricus terrestris*, and hemolytic lectin CEL-III from *Cucumaria echinata* (*48*, *49*). These proteins utilize a β-trefoil domain to bind carbohydrates. These proteins contain multiple carbohydrate binding sites, some of which use tryptophan residues to coordinate sugars, while other sites are coordinated using charged residues that can stack with a tyrosine residue. Thus, the botulinum toxins and tetanus toxin are unique prokaryotic proteins that use a β-trefoil domain and a tryptophan residue to bind gangliosides, which have a binding strategy similar to that of the eukaryotic lectins.

Structure of HCR/D-SA and Vaccine Properties. BoNTs are category A select agents because of their extreme potency and duration of paralysis in humans. Though not associated with natural human intoxication, BoNT/C and BoNT/D are toxic in mammalian neuronal tissue (*50*) and BoNT/C causes paralysis in human neuromuscular preparations (*23*) and has been implicated as an agent for human therapy (*51*). In addition, there is interest in developing a multiserotype vaccine capable of neutralizing all BoNT serotypes. Traditional vaccination strategies use formaldehyde-inactivated BoNT, where toxicity is eliminated, but immunogenicity is retained (*30*). An alternative vaccine strategy utilizes immunization with recombinant HCRs. The recombinant HCRs can be produced in large quantities and are free of neurotoxin contamination. Mice immunized with a cocktail of HCR domains of the seven prototypical serotypes (HCR/A−G) were resistant to challenge by each neurotoxin (BoNT/A−G), demonstrating the efficacy of this strategy (*52*). In addition, antisera from mice immunized with the hepta-serotype HCR vaccine blocked binding of HCRs to gangliosides in vitro (*41*). These studies indicate neutralizing antibodies interfere with receptor recognition. Atassi and colleagues utilized a peptide array and identified immune reactive epitopes adjacent to the ganglioside and protein receptor binding regions of the HCR domain (*53*, *54*). Interestingly, antibodies were not detected that were directed against the GBP, which suggests that the ganglioside pocket does not represent an efficient neutralization site. One caveat to this interpretation is that neutralizing epitopes may be composed of discontinuous segments of the peptide chain that become juxtaposed following protein folding which would preclude detection by peptide array analysis.

Unlike the ganglioside binding pocket, the GBL of BoNT/C and BoNT/D-SA is a β-hairpin loop that protrudes from the HCR. The lack of cross protection observed by mice immunized with HCR/C upon challenge with BoNT/D-SA indicates the neutralizing epitopes are not conserved between these two BoNT subtypes, and thus, the β-loop may be a potential site for eliciting serotype specific neutralizing antibodies. Consistent with this region contributing to immune stimulation is the recent observation by Fairweather and co-workers, who reported that deletion of the GBL homologous region of HCR/TeNT reduced the capacity to elicit a neutralizing immune response (*55*). Studies are underway to determine the role of the GBL in eliciting a protective response against botulism.

ACKNOWLEDGMENT

We acknowledge the assistance of Amanda Przedpelski for HCR production. We thank the staff at Advanced Photon Source beamline SBC 19ID for their excellent assistance in data collection. Results shown in this report are derived from work performed at Argonne National Laboratory, Structural Biology Center at the Advanced Photon Source. Argonne is operated by UChicago Argonne, LLC, for the U.S. Department of Energy, Office of Biological and Environmental Research under contract DE-AC02-06CH11357.

REFERENCES

1. Gill, D. M. (1982) Bacterial toxins: A table of lethal amounts. *Microbiol. Mol. Biol. Rev. 46*, 86–94.
2. Lacy, D. B., Tepp, W., Cohen, A. C., DasGupta, B. R., and Stevens, R. C. (1998) Crystal structure of botulinum neurotoxin type A and implications for toxicity. *Nat. Struct. Mol. Biol. 5*, 898–902.

3. Kumaran, D., Eswaramoorthy, S., Furey, W., Navaza, J., Sax, M., and Swaminathan, S. (2009) Domain Organization in *Clostridium botulinum* Neurotoxin Type E Is Unique: Its Implication in Faster Translocation. *J. Mol. Biol. 386*, 233–245.
4. Montecucco, C., and Schiavo, G. (1995) Structure and function of tetanus and botulinum neurotoxins. *Q. Rev. Biophys. 28*, 423–472.
5. Montecucco, C., and Schiavo, G. (1993) Tetanus and botulism neurotoxins: A new group of zinc proteases. *Trends Biochem. Sci. 18*, 324–327.
6. Brunger, A. T., Breidenbach, M. A., Jin, R., Fischer, A., Santos, J. S., and Montal, M. (2007) Botulinum Neurotoxin Heavy Chain Belt as an Intramolecular Chaperone for the Light Chain. *PLoS Pathog. 3*, e113.
7. Verderio, C., Rossetto, O., Grumelli, C., Frassoni, C., Montecucco, C., and Matteoli, M. (2006) Entering neurons: Botulinum toxins and synaptic vesicle recycling. *EMBO Rep. 7*, 995–999.
8. Ochanda, J. O., Syuto, B., Ohishi, I., Naiki, M., and Kubo, S. (1986) Binding of *Clostridium botulinum* Neurotoxin to Gangliosides. *J. Biochem. 100*, 27–33.
9. Dong, M., Yeh, F., Tepp, W. H., Dean, C., Johnson, E. A., Janz, R., and Chapman, E. R. (2006) SV2 Is the Protein Receptor for Botulinum Neurotoxin A. *Science 312*, 592–596.
10. Dong, M., Tepp, W. H., Liu, H., Johnson, E. A., and Chapman, E. R. (2007) Mechanism of botulinum neurotoxin B and G entry into hippocampal neurons. *J. Cell Biol. 179*, 1511–1522.
11. Dong, M., Richards, D. A., Goodnough, M. C., Tepp, W. H., Johnson, E. A., and Chapman, E. R. (2003) Synaptotagmins I and II mediate entry of botulinum neurotoxin B into cells. *J. Cell Biol. 162*, 1293–1303.
12. Dong, M., Liu, H., Tepp, W. H., Johnson, E. A., Janz, R., and Chapman, E. R. (2008) Glycosylated SV2A and SV2B Mediate the Entry of Botulinum Neurotoxin E into Neurons. *Mol. Biol. Cell 19*, 5226–5237.
13. Fu, Z., Chen, C., Barbieri, J. T., Kim, J.-J. P., and Baldwin, M. R. (2009) Glycosylated SV2 and Gangliosides as Dual Receptors for Botulinum Neurotoxin Serotype F. *Biochemistry 48*, 5631–5641.
14. Montal, M. (2009) Translocation of botulinum neurotoxin light chain protease by the heavy chain protein-conducting channel. *Toxicon 54*, 565–569.
15. Fischer, A., and Montal, M. (2007) Single molecule detection of intermediates during botulinum neurotoxin translocation across membranes. *Proc. Natl. Acad. Sci. U.S.A. 104*, 10447–10452.
16. Fischer, A., and Montal, M. (2007) Crucial Role of the Disulfide Bridge between Botulinum Neurotoxin Light and Heavy Chains in Protease Translocation across Membranes. *J. Biol. Chem. 282*, 29604–29611.
17. Schiavo, G. G., Benfenati, F., Poulain, B., Rossetto, O., de Laureto, P. P., DasGupta, B. R., and Montecucco, C. (1992) Tetanus and botulinum-B neurotoxins block neurotransmitter release by proteolytic cleavage of synaptobrevin. *Nature 359*, 832–835.
18. Binz, T., Blasi, J., Yamasaki, S., Baumeister, A., Link, E., Südhof, T. C., Jahn, R., and Niemann, H. (1994) Proteolysis of SNAP-25 by types E and A botulinal neurotoxins. *J. Biol. Chem. 269*, 1617–1620.
19. Yamasaki, S., Baumeister, A., Binz, T., Blasi, J., Link, E., Cornille, F., Roques, B., Fykse, E. M., SÃ1/4dhof, T. C., and Jahn, R. (1994) Cleavage of members of the synaptobrevin/VAMP family by types D and F botulinal neurotoxins and tetanus toxin. *J. Biol. Chem. 269*, 12764–12772.
20. Blasi, J., Chapman, E. R., Yamasaki, S., Binz, T., Niemann, H., and Jahn, R. (1993) Botulinum neurotoxin C1 blocks neurotransmitter release by means of cleaving HPC-1/syntaxin. *EMBO J. 12*, 4821–4828.
21. Oguma, K., Yokota, K., Hayashi, S., Takeshi, K., Kumagai, M., Itoh, N., Tachi, N., and Chiba, S. (1990) Infant botulism due to *Clostridium botulinum* type C toxin. *Lancet 336*, 1449–1450.
22. Gangarosa, E. J., Donadio, J. A., Armstrong, R. W., Meyer, K. F., Brachman, P. S., and Dowell, V. R. (1971) Botulism in the United States, 1899−1969. *Am. J. Epidemiol. 93*, 93–101.
23. Coffield, J. A., Bakry, N., Zhang, R. D., Carlson, J., Gomella, L. G., and Simpson, L. L. (1997) In vitro characterization of botulinum toxin types A, C and D action on human tissues: Combined electrophysiologic, pharmacologic and molecular biologic approaches. *J. Pharmacol. Exp. Ther. 280*, 1489–1498.
24. Neimanis, A., Gavier-Widen, D., Leighton, F., Bollinger, T., Rocke, T., and Morner, T. (2007) An outbreak of type C botulism in herring gulls (*Larus argentatus*) in southeastern Sweden. *J. Wildl. Dis. 43*, 327–336.
25. Davletov, B., Bajohrs, M., and Binz, T. (2005) Beyond BOTOX: Advantages and limitations of individual botulinum neurotoxins. *Trends Neurosci. 28*, 446–452.
26. Brand, C. J., Schmitt, S. M., Duncan, R. M., and Cooley, T. M. (1988) An outbreak of type E botulism among common loons (*Gavia immer*) in Michigan's upper peninsula. *J. Wildl. Dis. 24*, 471–476.
27. Tsukamoto, K., Kohda, T., Mukamoto, M., Takeuchi, K., Ihara, H., Saito, M., and Kozaki, S. (2005) Binding of *Clostridium botulinum* Type C and D Neurotoxins to Ganglioside and Phospholipid. *J. Biol. Chem. 280*, 35164–35171.
28. Baldwin, M. R., and Barbieri, J. T. (2007) Association of Botulinum Neurotoxin Serotypes A and B with Synaptic Vesicle Protein Complexes. *Biochemistry 46*, 3200–3210.
29. Rummel, A., Hafner, K., Mahrhold, S., Darashchonak, N., Holt, M., Jahn, R., Beermann, S., Karnath, T., Bigalke, H., and Binz, T. (2009) Botulinum neurotoxins C, E and F bind gangliosides via a conserved binding site prior to stimulation-dependent uptake with botulinum neurotoxin F utilising the three isoforms of SV2 as second receptor. *J. Neurochem. 110*, 1942–1954.
30. Webb, R. P., Smith, T. J., Wright, P. M., Montgomery, V. A., Meagher, M. M., and Smith, L. A. (2007) Protection with recombinant *Clostridium botulinum* C1 and D binding domain subunit (Hc) vaccines against C and D neurotoxins. *Vaccine 25*, 4273–4282.
31. Chen, C., Fu, Z., Kim, J.-J. P., Barbieri, J. T., and Baldwin, M. R. (2009) Gangliosides as High Affinity Receptors for Tetanus Neurotoxin. *J. Biol. Chem. 284*, 26569–26577.
32. Minor, W., Tomchick, D., and Otwinowski, Z. (2000) Strategies for macromolecular synchrotron crystallography. *Structure 8*, R105–R110.
33. Collaborative Computational Project Number 4 (1994) The CCP4 suite: Programs for protein crystallography. *Acta Crystallogr. D50*, 760–763.
34. Brunger, A. T. (2007) Version 1.2 of the Crystallography and NMR system. *Nat. Protoc. 2*, 2728–2733.
35. Roussel, A., Fontecilla-Camps, J. C., and Cambillau, C. (1990) CRYStallize: A crystallographic symmetry display and handling subpackage in TOM/FRODO. *J. Mol. Graphics 8*, 86–88.
36. Moriishi, K., Koura, M., Abe, N., Fujii, N., Fujinaga, Y., Inoue, K., and Ogumad, K. (1996) Mosaic structures of neurotoxins produced from *Clostridium botulinum* types C and D organisms. *Biochim. Biophys. Acta 1307*, 123–126.
37. Jin, R., Rummel, A., Binz, T., and Brunger, A. T. (2006) Botulinum neurotoxin B recognizes its protein receptor with high affinity and specificity. *Nature 444*, 1092–1095.
38. Chai, Q., Arndt, J. W., Dong, M., Tepp, W. H., Johnson, E. A., Chapman, E. R., and Stevens, R. C. (2006) Structural basis of cell surface receptor recognition by botulinum neurotoxin B. *Nature 444*, 1096–1100.
39. Stenmark, P., Dupuy, J., Imamura, A., Kiso, M., and Stevens, R. C. (2008) Crystal structure of botulinum neurotoxin type A in complex with the cell surface co-receptor GT1b: Insight into the toxin-neuron interaction. *PLoS Pathog. 4*, e1000129.
40. Rummel, A., Mahrhold, S., Bigalke, H., and Binz, T. (2004) The HCC-domain of botulinum neurotoxins A and B exhibits a singular ganglioside binding site displaying serotype specific carbohydrate interaction. *Mol. Microbiol. 51*, 631–643.
41. Chen, C., Baldwin, M. R., and Barbieri, J. T. (2008) Molecular Basis for Tetanus Toxin Coreceptor Interactions. *Biochemistry 47*, 7179–7186.
42. Tsukamoto, K., Kozai, Y., Ihara, H., Kohda, T., Mukamoto, M., Tsuji, T., and Kozaki, S. (2008) Identification of the receptor-binding sites in the carboxyl-terminal half of the heavy chain of botulinum neurotoxin types C and D. *Microb. Pathog. 44*, 484–493.
43. Nuemket, N., Tanaka, Y., Tsukamoto, K., Tsuji, T., Nakamura, K., Kozaki, S., Yao, M., and Tanaka, I. (2010) Preliminary X-ray crystallographic study of the receptor-binding domain of the D/C mosaic neurotoxin from *Clostridium botulinum*. *Acta Crystallogr. F66*, 608–610.
44. Lacy, D. B., and Stevens, R. C. (1999) Sequence homology and structural analysis of the clostridial neurotoxins. *J. Mol. Biol. 291*, 1091–1104.
45. Merritt, E. A., Sarfaty, S., Akker, F. v. d., L'Hoir, C., Martial, J. A., and Hol, W. G. (1994) Crystal structure of cholera toxin B-pentamer bound to receptor GM1 pentasaccharide. *Protein Sci. 3*, 166–175.
46. Zhang, R. G., Scott, D. L., Westbrook, M. L., Nance, S., Spangler, B. D., Shipley, G. G., and Westbrook, E. M. (1995) The three-dimensional crystal structure of cholera toxin. *J. Mol. Biol. 251*, 563–573.
47. Varghese, J. N., McKimm-Breschkin, J. L., Caldwell, J. B., Kortt, A. A., and Colman, P. M. (1992) The structure of the complex between influenza virus neuraminidase and sialic acid, the viral receptor. *Proteins 14*, 327–332.
48. Maveyraud, L., Niwa, H., Guillet, V., Svergun, D. I., Konarev, P. V., Palmer, R. A., Peumans, W. J., Rouge, P., Van Damme, E. J., Reynolds, C. D., and Mourey, L. (2009) Structural basis for sugar recognition, including the Tn carcinoma antigen, by the lectin SNA-II from *Sambucus nigra*. *Proteins 75*, 89–103.
49. Hatakeyama, T., Unno, H., Kouzuma, Y., Uchida, T., Eto, S., Hidemura, H., Kato, N., Yonekura, M., and Kusunoki, M. (2007)

C-type lectin-like carbohydrate recognition of the hemolytic lectin CEL-III containing ricin-type β-trefoil folds. *J. Biol. Chem. 282*, 37826–37835.
50. Kalandakanond, S., and Coffield, J. A. (2001) Cleavage of intracellular substrates of botulinum toxins A, C, and D in a mammalian target tissue. *J. Pharmacol. Exp. Ther. 296*, 749–755.
51. Eleopra, R., Tugnoli, V., Rossetto, O., Montecucco, C., and De Grandis, D. (1997) Botulinum neurotoxin serotype C: A novel effective botulinum toxin therapy in human. *Neurosci. Lett. 224*, 91–94.
52. Baldwin, M. R., Tepp, W. H., Przedpelski, A., Pier, C. L., Bradshaw, M., Johnson, E. A., and Barbieri, J. T. (2008) Subunit vaccine against the seven serotypes of botulism. *Infect. Immun. 76*, 1314–1318.
53. Dolimbek, B. Z., Steward, L. E., Aoki, K. R., and Atassi, M. Z. (2008) Immune recognition of botulinum neurotoxin B: Antibody-binding regions on the heavy chain of the toxin. *Mol. Immunol. 45*, 910–924.
54. Dolimbek, B. Z., Aoki, K. R., Steward, L. E., Jankovic, J., and Atassi, M. Z. (2007) Mapping of the regions on the heavy chain of botulinum neurotoxin A (BoNT/A) recognized by antibodies of cervical dystonia patients with immunoresistance to BoNT/A. *Mol. Immunol. 44*, 1029–1041.
55. Qazi, O., Sesardic, D., Tierney, R., Soderback, Z., Crane, D., Bolgiano, B., and Fairweather, N. (2006) Reduction of the ganglioside binding activity of the tetanus toxin HC fragment destroys immunogenicity: Implications for development of novel tetanus vaccines. *Infect. Immun. 74*, 4884–4891.